Supplementary Information (SI) for Sustainable Energy & Fuels.

- Supporting Information -

Nitrate reduction to ammonia using Cu-Fe nanoparticles

Ido Dan[1], Paz Stein[1], Dyuti Bandyopadhyay[1], Yan Tetarevsky[1], Alevtina Neyman[1], Shir Abramovich[1], Rotem Geva[1], Maya Bar Sadan[1*]

[1] Department of chemistry, Ben Gurion University, Beer-Sheva, 8410501 Israel.

* barsadan@bgu.ac.il

Materials:

Iron(III) chloride hexahydrate ($FeCl_3 \cdot 6H_2O$ 97%, Sigma Aldrich), Sodium borohydride ($NaBH_4$ 99%, Sigma Aldrich), Copper(II) chloride ($CuCl_2$ 99%, Sigma Aldrich). Di-sodium hydrogen phosphate anhydrous (Na_2HPO_4), sodium phosphate monobasic anhydrous (NaH_2PO_4), obtained from Glentham Life Sciences. sodium chloride (NaCl 99.5%, Sigma Aldrich). Salicylic acid (99%) and trisodium citrate dihydrate (99%) were obtained from Alfa Aesar). Sodium nitroprusside dihydrate (>99%, Sigma Aldrich), Sulfanilamide (99%, Aaron Chemicals), n-1-naphtylethylene diamine dihydrochloride (Fisher Chemicals). Nafion D-521 dispersion (5 %w/w) and sodium hypochlorite (11-14% available chlorine) were obtained from Alfa Aesar. Sodium nitrate ($NaNO_3$) sodium nitrite ($NaNO_2$), analysis grade (Supelco) and ammonium chloride (NH_4Cl, 99.5% Acros Organics) were freeze-dried overnight and kept in a glove box prior to usage. Sodium hydroxide and isopropyl alcohol were purchased from Bio-Lab Ltd. Ethanol was obtained from ROMICAL. The water used for any of the experiments were de-ionized and purified by a Millipore Milli-Q purification setup with resistance over 18.2 MΩ

Electrochemical measurements

The electrocatalytic experiments were performed using BioLogic VSP workstation in an H-type cell, where the two compartments were separated by a Nafion 117 membrane. The Nafion 117 membranes were pre-treated by sequential immersion in gently boiling 3% H_2O_2 (1 h), deionized water (2 h), and 0.5 M H_2SO_4 (1 h). Membranes were rinsed with hot deionized water after each step and stored in deionized water until use.[1] To prepare the catalyst ink, 1 mg of catalyst was mixed with 1 mg of carbon black (Vulcan XC 72R, Fuel Cell Store, USA), 200 μL of deionized water, 200 μL of isopropanol, and 15 μL of Nafion solution. Carbon black was incorporated to enhance the conductivity of the catalyst layer and to improve the dispersion of catalyst particles, ensuring optimal electrochemical performance. The catalyst ink was sonicated in an ultrasonic bath for 30 minutes, followed by probe sonication using a QSonica Q125 instrument (pulse rate 10/5 s, 40% amplitude) for a total of 5 minutes. A 15 µL aliquot of the ink (containing 36 µg catalyst) was drop-cast onto a 3 mm diameter glassy carbon electrode (CHI-104, CH Instruments, Inc.) and air-dried for 24 hours prior to use. An Ag/AgCl reference electrode in saturated KCl (013691 RE-1CP, ALS, Japan) and a Pt foil counter electrode (Gaoss Union) were employed in the setup. A 0.1 M phosphate-buffered saline (PBS) solution served as the electrolyte for control experiments, while a 0.1 M PBS/$NaNO_3$ solution was used for nitrate reduction (NO_3RR) activity measurements. Prior to and during the electrochemical measurements, both cell compartments were purged with 99.999% argon for 15 minutes, and the cathodic chamber was continuously stirred.

In this work, all potentials were converted from Ag|AgCl saturated KCl reference to relative to reversible hydrogen electrode (RHE), using the following calculation:

$$E_{RHE} = E_{(Ag|AgCl)} + E^{0}_{(Ag|AgCl\,)} + 0.059 \cdot pH$$

Where $E^0_{(Ag|AgCl)}$ value is 0.197 V, and the electrolyte pH was measured using a calibrated pH meter.

The faradaic efficiency of NH_3 and NO_2^- was calculated as follows:

$$FE = \frac{z \cdot C \cdot V \cdot F}{Q} \times 100\%$$

Where z is the number of electrons transferred in the reaction, 8 for NH_3 production and 2 for NO_2^-, C is the product's concentration (mol L^{-1}), V is the electrolyte volume in the cathodic compartment (0.035 L), F is Faraday constant (96,485 C mol^{-1}), and Q is the total charge passed during the measurement (C).

NH_3 yield rate was calculated by:

$$r_{NH_3} = \frac{C \cdot V \cdot Mw_{NH_3}}{t \cdot m_{catalyst}}$$

Where Mw_{NH3} is the molecular weight of ammonia (17 g mol^{-1}), t is the measurement duration (hours), and $m_{catalyst}$ is the catalyst loading mass (mg).

Characterization Setups

Transmission electron microscopy (TEM) samples were prepared by dispersing the catalyst powder in ethanol by ultrasonication, and then drop casting ~20 µL on a Cu grid (300 mesh, TED PELLA, INC). Images were acquired by Tecnai T12 G^2 TWIN Thermo Fisher transmission electron microscope.

High-resolution transmission electron microscopy (HRTEM) imaging was acquired using double aberration-corrected Themis Z microscope (Thermo FisherScientific Electron Microscopy Solutions, Hillsboro, USA) with a high-brightness FEG and applied voltage of 200 kV. High-angle-annular dark-field (HAADF) scanning transmission electron microscopy (STEM) images were acquired using a Fischione Model 3000 detector with a semi-convergence angle of 21 mrad, a probe current of 50 pA, and an inner collection angle of 60.0 mrad.

Scanning Electron Microscopy (SEM) samples were prepared by drop casting the dispersed catalyst in ethanol onto a Si wafer. Images were acquired using a Verios-460L field-emission scanning electron microscope from Thermo Fisher.

Powder X-ray diffraction (XRD) patterns were collected using a Panalytical Emyrean X-ray diffractometer with a position-sensitive X'Celerator detector and a Cu Kα (λ = 1.5405 Å) X-ray source, operated at 40 kV and 30 mA.

X-ray photoelectron spectroscopy (XPS) measurements were carried out with ESCALAB 250 spectrometer under ultrahigh vacuum (1×10^{-9} bar) apparatus with an Al Kα X-ray radiating source and a monochromator.

UV-Vis absorbance was measured using SHIMADZU UV-3600 UV-vis-NIR spectrophotometer in 10 mm square polystyrene cuvettes. Measurements were acquired for 400-800 nm wavelength range.

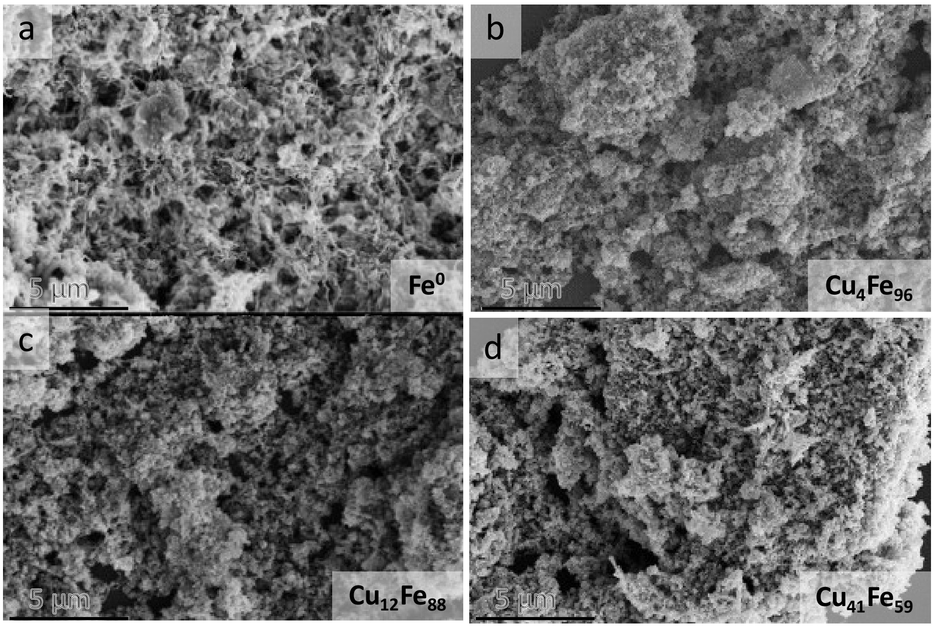

Figure S1. SEM images of **(a)** Fe particles, and Cu-doped Fe particles with 4%, 12%, 41% Cu content (**b-d** respectively).

$Cu_{99}Fe_1$ synthesis and characterization

When Fe particles were reacted with an excess of Cu^{2+} (Cu molar ratio of 4:1), nearly complete galvanic replacement occurred, forming particles composed of approximately 99% copper and resulting in cube-like structures around 600 nm in size **(Figure S2a-b)**. The O 1s spectrum showed contributions only from hydroxyl groups on the surface, consistent with the relatively small amount of Cu^{2+} present on the surface, as evident from the corresponding Cu 2p spectrum **(Figure S2c)**. For this sample with a high Cu content, peaks corresponding to CuCl were detected in the XRD pattern, while the signal for Fe disappeared (**Figure S2d**). The LSV curves of the $Cu_{99}Fe_1$ particles closely resemble the ones of CuCl salt. Chronoamperometric experiments conducted at 0.9 V further support this, showing similar ammonia production activity (**Figure S3**).

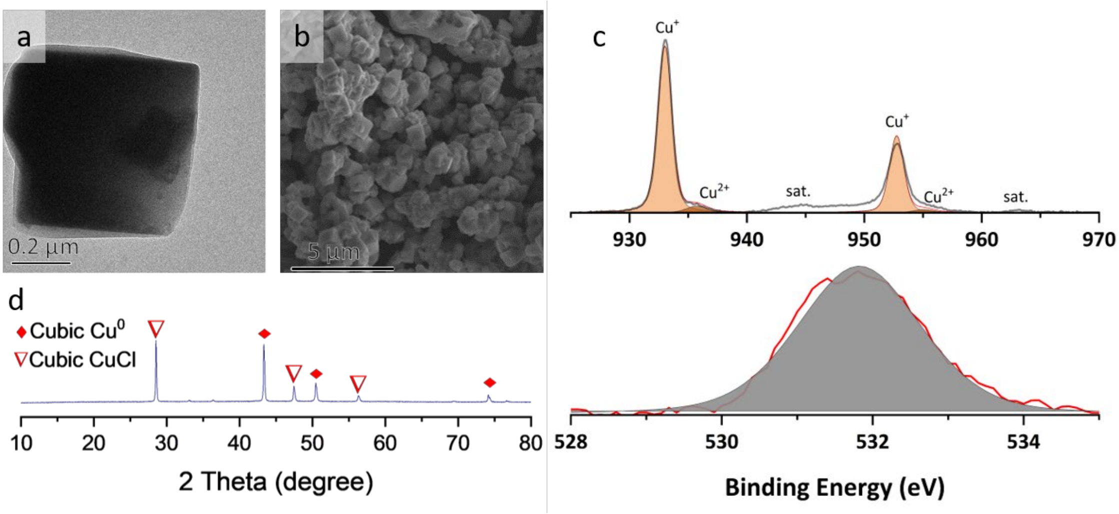

Figure S2. Characterization of $Cu_{99}Fe_1$ particles: **(a)** TEM and **(b)** SEM images, **(c)** XPS spectra of Cu 2p (top) and O 1s (bottom) regions, and **(d)** XRD pattern.

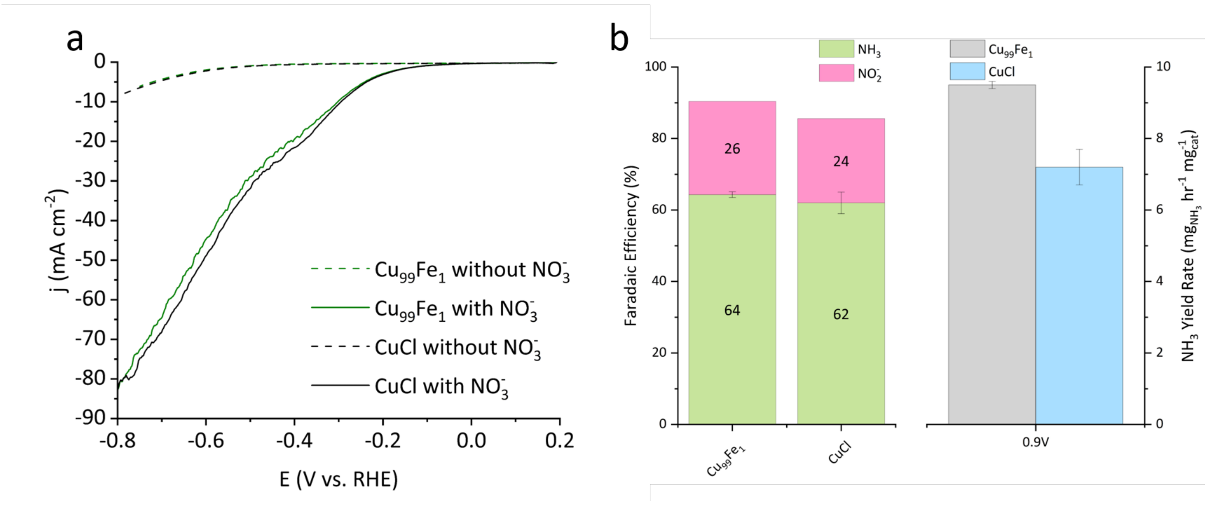

Figure S3. Electrochemical NO_3RR of $Cu_{99}Fe_1$ particles and CuCl. **(a)** Linear scan voltammograms in 0.1M PBS, with and without of 0.1 M $NaNO_3$. **(b)** Faradaic efficiency values for NH_3 and NO_2^- formation and ammonia yield rates after applying 5 Coulombs per at 0.9V.

Table S1. X-ray photoelectron spectroscopy binding energies of Cu-Fe particles

Element	Species	Binding Energy	Reference
Fe $2p_{3/2}$	Fe^0	707.0-707.6	[2]
	Fe^{+2}	710.8-711.3	[4 ,3]
	Fe^{+3}	714.0-714.8	[4 ,3]
Fe $2p_{1/2}$	Fe^0	720.4-720.9	[2]
	Fe^{+2}	724.0-725.0	[3]
	Fe^{+3}	726.9-727.6	[3]
Fe $2p_{3/2}$ (satellite)		718.5-719.5	
		722.2	
Fe $2p_{1/2}$ (satellite)		731.3-732.1	
		734.9	
Cu $2p_{3/2}$	Cu^{+1}	932.0-933.2	[5, 6]
	Cu^{+2}	933.9-935.7	[5, 6]
Cu $2p_{1/2}$	Cu^{+1}	952.5-952.7	[5, 6]
	Cu^{+2}	954.0-955.1	[5, 6]
Cu $2p_{3/2}$ (satellite)		939.7-941.5	[6]
		943.2-944.3	[6]
Cu $2p_{1/2}$ (satellite)		962.2-962.2	[6]
		963.0-963.6	[6]
O 1s	metallic oxide M-O	529.9-930.4	[4-6]
	hydroxyl group -OH	531.3-531.8	[6]

The oxidation state of Cu was determined using the Cu LMM Auger spectra, as shown in **Figure S4a-c**. In the Cu_4Fe_{96} sample (**Figure S4a**), a peak at 570.5 eV indicates a predominant presence of the Cu^+ state. Similarly, for the $Cu_{12}Fe_{88}$ sample (**Figure S4b**), a peak at 916.9 eV also confirms the Cu^+ state. However, in the $Cu_{41}Fe_{59}$ sample (**Figure S4c**), two distinct peaks at 570.0 eV and 568.3 eV suggest the presence of both Cu^+ and Cu^{2+} states. These observations corroborate the assignment of the lower doublet peaks in the Cu 2p spectra to the Cu^+ state, consistent with values reported in the literature.[7, 8]

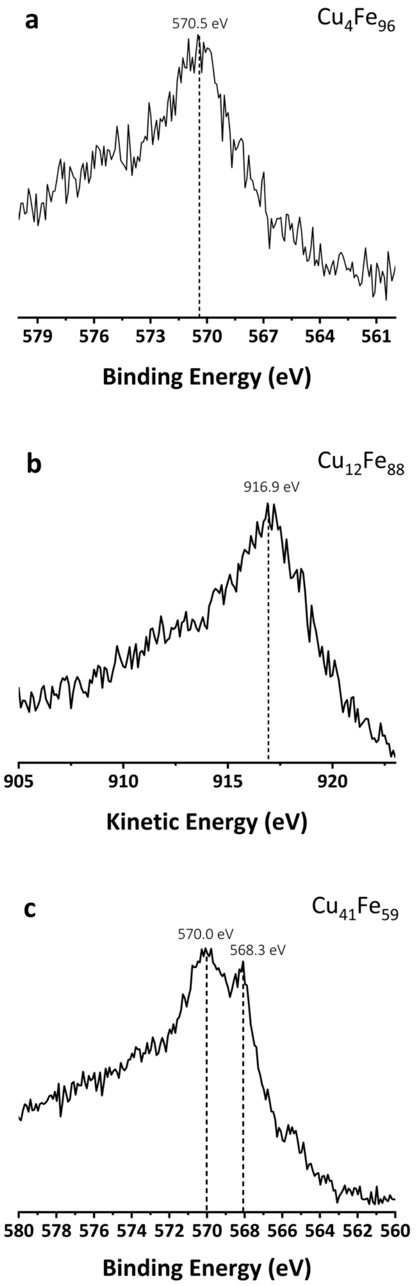

Figure S4. Cu LMM Auger spectra of **(a)** Cu_4Fe_{96}, **(b)** $Cu_{12}Fe_{88}$, and **(c)** $Cu_{41}Fe_{59}$ samples.

Colorimetric Determination of NH_4^+ and NO_2^-

NH_4^+ concentration was determined using the indophenol blue method and the absorbance was measured at 655 nm.[9] Samples were prepared by mixing 0.5 mL of appropriately diluted electrolyte solution with 0.5 mL of 1 M NaOH solution containing 5%w/w of salicylic acid and 5%w/w trisodium citrate. Then, 0.5 mL of 0.05 M NaClO and 0.05 mL of 1%w/w sodium nitroprusside ($C_5FeN_6Na_2O$) were added, and the samples were mixed and let for color development for 2 hours.

The concentration of NO_2^- was determined using the Griess test and the absorbance was measured at 540 nm. Color reagent was prepared by dissolving 0.5 g of sulfanilamide and 0.5 g of N-1-naphtylethylenediamine dihydrochloride in 50 mL of deionized water. Samples were prepared by mixing 0.5 mL of appropriately diluted electrolyte with 1 mL of DIW and 0.5 mL of Griess color reagent and let for color development for 20 minutes.

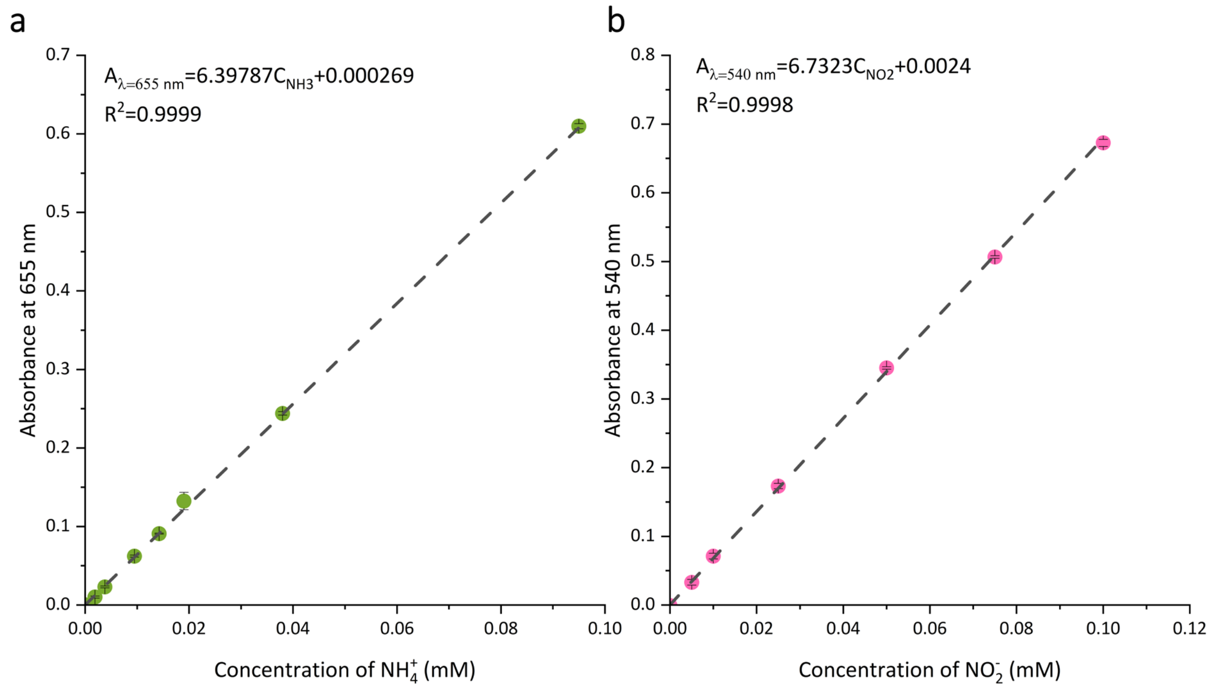

Figure S5. calibration curve of **(a)** NH_4^+ and **(b)** NO_2^- in 0.1 M PBS/NO_3^-.

Determination of NH_4^+ concentration by ^1H NMR

The concentrations of the electrochemically produced $^{14}NH_4^+$ and $^{15}NH_4^+$ were determined using a Bruker AVANCE III-500 NMR instrument. Calibration curves were established with maleic acid ($C_4H_4O_4$) as the internal standard, using ammonium standards ranging from 200 to 500 μM.[9] Samples were prepared by mixing 280 μL of electrolyte, 20 μL of 8.5 mM maleic acid, 13 μL of concentrated H_2SO_4, and 100 μL of DMSO-d_6. After water suppression by presaturation, the solution was analyzed using ^1H NMR to determine $^{15}NH_4^+$ or $^{14}NH_4^+$ concentrations.

The $^{14}NH_4^+$ products of the chronoamperometric experiments exhibited a ^1H NMR triplet centered around 6.80, 6.90, and 7.00 ppm, while $^{15}NH_4^+$ displayed a doublet with picks at 6.83 and 6.97 ppm. Also, small peaks that align with the $^{14}NH_4^+$ triplet are observed in the $^{15}NH_4^+$ spectrum, these were too weak for integration and could be a result of trace $^{14}NH_4^+$ in the electrochemical cell.

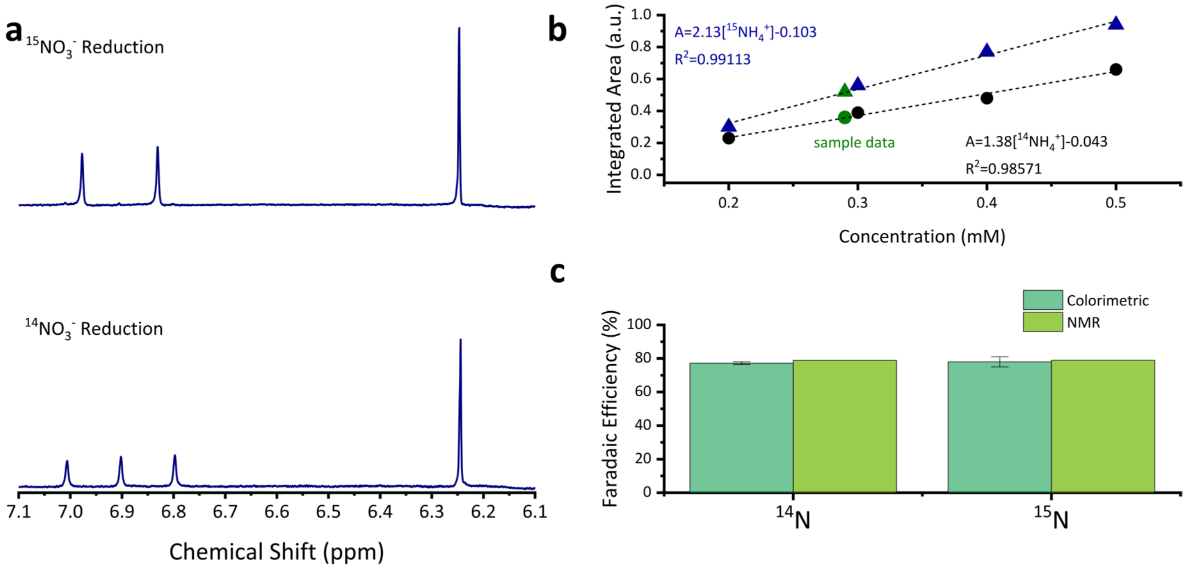

Figure S6. (a) ^1H nuclear magnetic resonance (NMR) spectra of NO_3RR products using $^{14}NO_3^-$ and $^{15}NO_3^-$ as sources. **(b)** ^1H-NMR calibration curves, calculated integrated area measured against maleic acid as internal standard. **(c)** calculated Faradaic efficiency values using colorimetric and NMR methods.

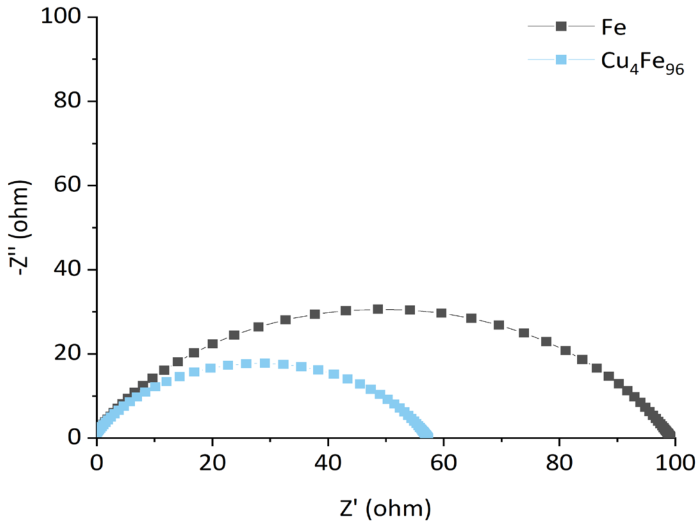

Figure S7. Electrochemical impedance spectroscopy (EIS) Nyquist plots of Fe and Cu_4Fe_{96} catalysts performed at -0.7 V vs RHE in 0.1 M PBS/NO_3^- electrolyte.

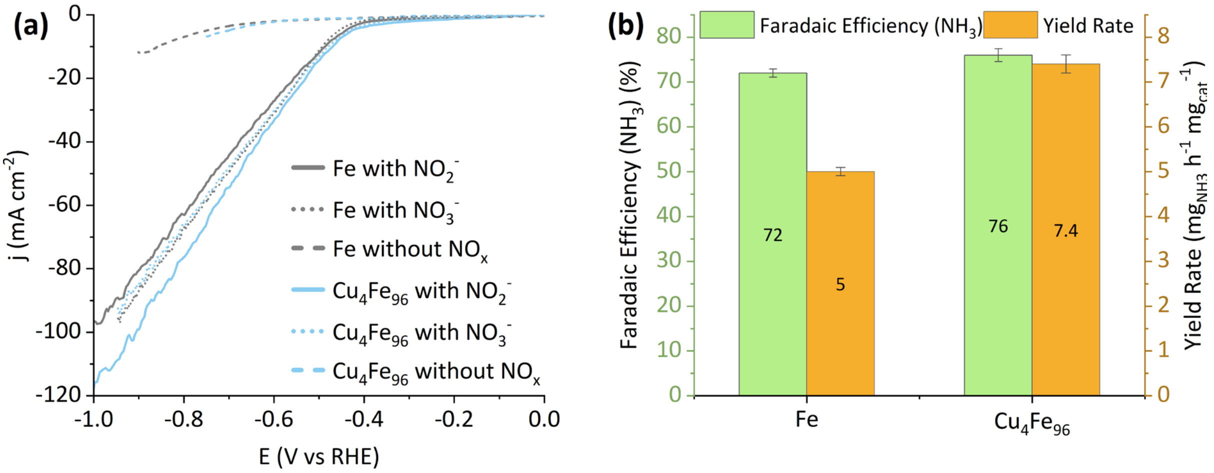

Figure S8. Electrochemical nitrite reduction performance of Fe and Cu_4Fe_{96} catalysts in 0.1 M PBS. **(a)** Linear sweep voltammetry (LSV) curves measured in electrolytes with 0.1 M NO_2^- (solid lines), without NO_x (dashed lines), and with 0.1 M NO_3^- (dotted lines), **(b)** Faradaic efficiency and NH_3 yield rate obtained from chronoamperometry at -0.7 V vs. RHE.

Table S2. Electrochemical NH_3 production performance comparison

Material	**Substrate**	**Electrolyte**	**Faradaic efficiency (%)**	**NH_3 yield rate (mg NH_3 hr^{-1} mg cat^{-1})**	**NH_3 yield rate (mg NH_3 h^{-1} cm^{-2})**	**V vs RHE (v)**	**Reference**
Fe	glassy carbon	0.1 M PBS, 0.1 M $NaNO_3$	77±1	9.9±0.2	5.1±0.1	-0.9	This work
Cu_4Fe_{96}			78.3±0.4	11.53±0.08	5.91±0.04		
$Cu_{12}Fe_8$			73±1	9.4±0.2	4.8±0.1		
$Cu_{41}Fe_{59}$			62±1	9.9±0.5	5.1±0.2		
Fe@CB	glassy carbon	0.1 M Na_2SO_4, 0.450 M $NaNO_3$	60.5			-0.7	[10]
Fe_2O_3	carbon cloth	0.5 M Na_2SO_4, 0.1 M $NaNO_3$	84.87		5.59 ± 0.39	−0.9	[11]
Cu–Fe_2O_3 nanotube arrays		0.5 M Na_2SO_4, 50 ppm NO^{3-}	80.1		1.84	-0.6	[12]
Cu_1-Fe	glassy carbon	0.1 M K_2SO_4, 50 mg L^{-1} KNO_3	95.4	3.1	1.98	-1.3	[13]
$Cu_{49}Fe_1$	glassy carbon	0.1 M K_2SO_4, 2 mM KNO_3	94.5	0.78	3.92	-0.74	[14]
Cu/Cu_2O nanowire arrays		0.5 M Na_2SO_4, 200 ppm NO^{3-}	95.8		4.17	-0.85	[15]
Cu mesh		0.5 M Na_2SO_4, 200 ppm NO^{3-}	39.8		0.46	-0.85	[15]
Cu nanowire arrays		0.5 M Na_2SO_4, 200 ppm NO^{3-}	43.9		0.85	-0.85	[15]
Fe-Co nanoparticles	graphite	0.05 M Na_2SO_4, 100 ppm $NaNO_3$	58.2		0.248	-0.785	[16]

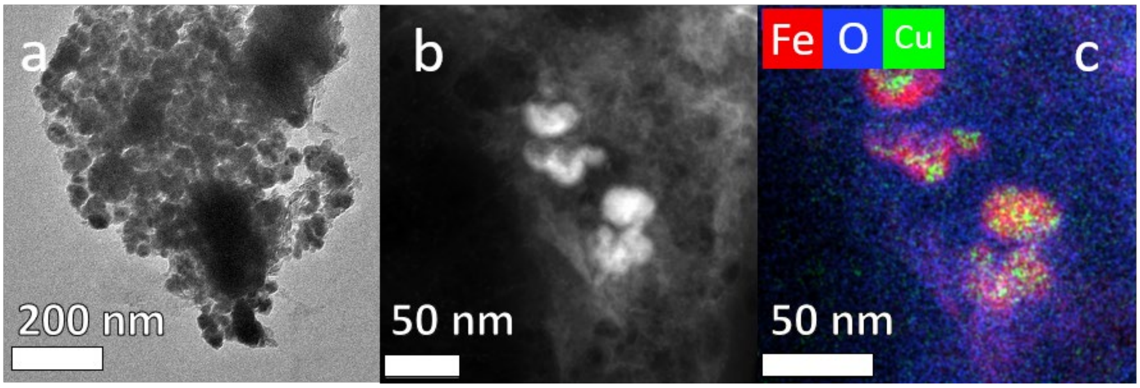

Figure S9. Electron microscopy analysis of post-NO_3RR Cu_4Fe_{96} particles: **(a)** TEM image, **(b)** STEM-HAADF, and **(c)** EDS elemental mapping.

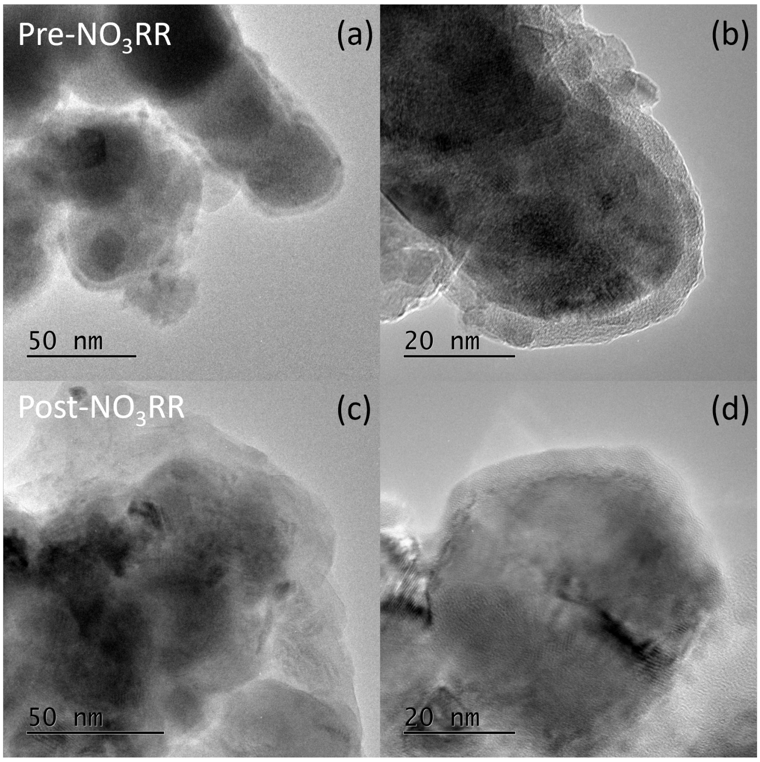

Figure S10. High resolution transmission electron microscopy (HRTEM) analysis of pre **(a-b)** and post-NO_3RR Cu_4Fe_{96} particles **(c-d).**

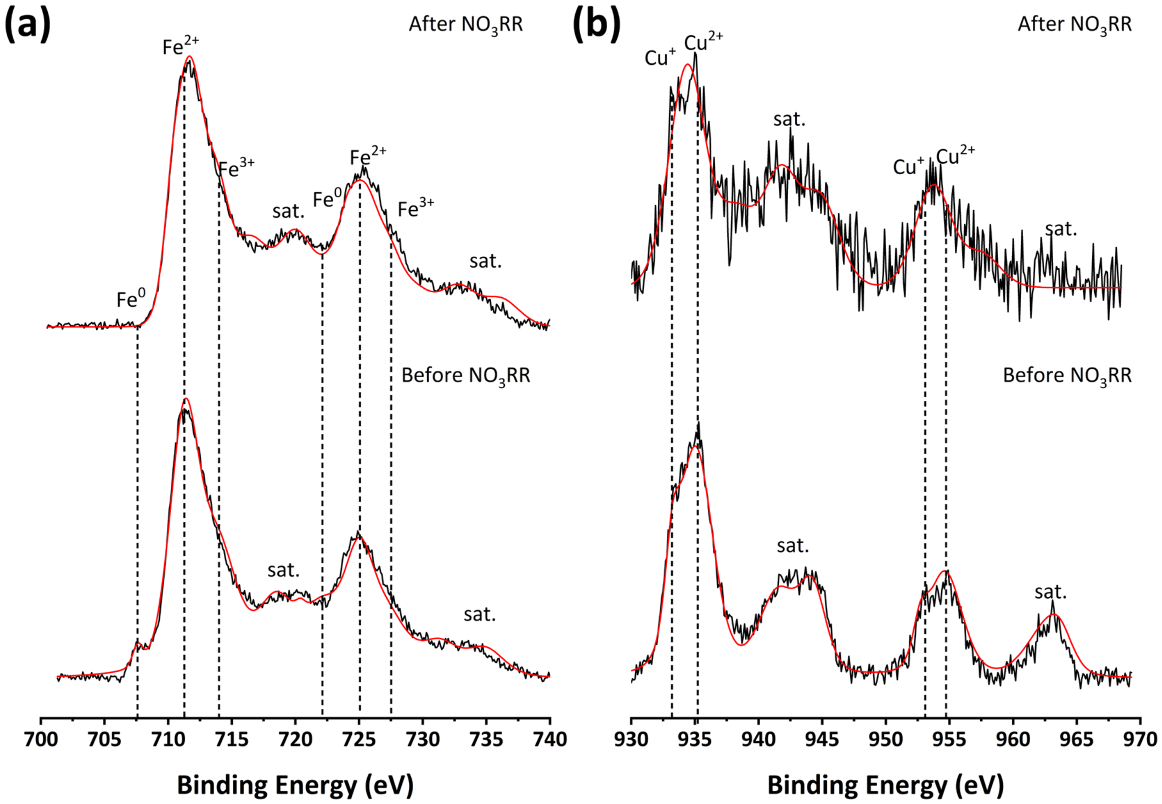

Figure S11. Comparison of XPS spectra of Cu_4Fe_{96} particles before and after NO_3RR: **(a)** Fe 2p and **(b)** Cu 2p.

References

1. Ticianelli, E.A., C.R. Derouin, and S. Srinivasan, *Localization of platinum in low catalyst loading electrodes to to attain high power densities in SPE fuel cells.* J. Electroanal. Chem. Interf. Electrochem., 1988. **251**(2): p. 275-295.

2. Tsuda, T., et al., *Iron phosphide nanocrystals as an air-stable heterogeneous catalyst for liquid-phase nitrile hydrogenation.* Nat. Commun., 2023. **14**(1): p. 5959.

3. Fan, Y.X., et al., *Enhancing* SO_2*-shielding effect and Lewis acid sites for high efficiency in low-temperature SCR of NO with* NH_3*: Reinforced electron-deficient extent of* Fe^{3+} *enabled by* Ti^{4+} *in* Fe_2O_3*.* Sep Purif Technol, 2023. **311**.

4. Reddy, G.K., P. Boolchand, and P.G. Smirniotis, *Unexpected Behavior of Copper in Modified Ferrites during High Temperature WGS Reaction-Aspects of Fe ⇆ Fe Redox Chemistry from Mossbauer and XPS Studies.* J. Phys. Chem. C, 2012. **116**(20): p. 11019-11031.

5. Xu, L., et al., *Comparison Study on the Stability of Copper Nanowires and Their Oxidation Kinetics in Gas and Liquid.* ACS Nano, 2016. **10**(3): p. 3823-3834.

6. Jiang, J.Y., et al., *Self-Supported Sheets-on-Wire CuO@Ni(OH)/Zn(OH) Nanoarrays for High-Performance Flexible Quasi-Solid-State Supercapacitor.* Processes, 2021. **9**(4).

7. Biesinger, M.C., *Advanced analysis of copper X-ray photoelectron spectra.* Surf. Interface Anal., 2017. **49**(13): p. 1325-1334.

8. Jang, J., et al., *Facile design of oxide-derived Cu nanosheet electrocatalyst for* CO_2 *reduction reaction.* EcoMat, 2023. **5**(5): p. e12334.

9. Stein, P., et al., *Copper-Based Nitrides Outperform Phosphides in Nitrate Electroreduction to Ammonia: The Cooperative Role of the* Cu_3N/CuO *Interface.* ChemCatChem, 2025. **17**(8): p. e202500156.

10. Feng, Y.R., et al., *Polarity Modulation Enhances Electrocatalytic Reduction of Nitrate by Iron Nanocatalysts.* ACS EST Eng, 2024. **4**(4): p. 928-937.

11. Li, T.S., et al., *Understanding first electron transfer kinetic process of electrochemical nitrate reduction to ammonia on* Fe_2O_3 *nanorods array.* Chem. Eng J, 2024. **485**.

12. Gao, Y.H., et al., *Interfacial engineering of Cu-FeO nanotube arrays with built-in electric field and oxygen vacancies for boosting the electrocatalytic reduction of nitrates.* Mater Adv, 2022. **3**(18): p. 7107-7115.

13. Zhou, B., et al., *Cu1-Fe Dual Sites for Superior Neutral Ammonia Electrosynthesis from Nitrate.* Angew. Chem. Int. Ed., 2024: p. e202406046.

14. Wang, C.H., et al., *Metasequoia-like Nanocrystal of Iron-Doped Copper for Efficient Electrocatalytic Nitrate Reduction into Ammonia in Neutral Media.* ChemSusChem, 2021. **14**(8): p. 1825-1829.

15. Wang, Y., et al., *Unveiling the Activity Origin of a Copper-based Electrocatalyst for Selective Nitrate Reduction to Ammonia.* Angew. Chem. Int. Ed., 2020. **59**(13): p. 5350-5354.

16. Kuznetsova, I., et al., *Enhancing efficiency of nitrate reduction to ammonia by Fe and Co nanoparticle-based bimetallic electrocatalyst.* Int. J. Mol. Sci., 2024. **25**(13): p. 7089.